A Simple and Cost-Effective Physical Distancing Violation Detector Using a Rotating Time of Flight Lidar

Dwi Hanto [a,*], Hendra Adinanta [a], Suryadi [a], Rini Khamimatul Ula [a], Mefina Yulias Rofianingrum [a], Imam Mulyanto [a], Bambang Widiyatmoko [a], Edi Kurniawan [a]

[a] Research Center for Physics, Indonesian Institute of Sciences (LIPI), South Tangerang 15314, Indonesia
Corresponding author: *dwi.hanto@lipi.go.id

Abstract— **In this work, a simple and cost-effective physical distancing violation detector using a commercial lidar has been developed. Our system comprises time of flight (ToF) lidar, mounted a stepper motor to rotate ToF Lidar and range an object on the top. We control a rotation of the stepper motor, record the distance between the object and the ToF Lidar by using a microcontroller, and analyze the measuring data using a computer program. This system can also indirectly estimate the distance between two objects by applying a simple vector operation. This paper successfully detects and evaluates the distance between two dummy objects placed with various configurations. We obtained the estimated distances using our proposed method nearly equal to the actual distances measured manually. In addition, our system has been tested to measure the physical distances among people with three volunteers who stood 200 cm and 80 cm distances in an indoor environment. The experiment results show that the distance between volunteer 1 and volunteer 2 is 186.5 cm and the distance between volunteer 2 and volunteer 3 is 73.0 cm. These indicate our system could provide information whether a safe distance or a risk distance. This research work can help the authorities provide an instrument for reducing contagious diseases, especially COVID-19 pandemic outbreaks, by installing at a fixed location or in portable instrument services.**

Keywords— **Lidar; physical distancing; pandemic.**

I. INTRODUCTION

World Health Organization (WHO) has announced the COVID-19 virus outbreak as a pandemic since 2020 [1]. The viruses were easily transmitted from the infected individual to other persons through respiratory droplets, especially when they are in close contact [2]. According to WHO and the Center for Disease Control and Prevention (CDC), respiratory droplets are believed to reach up to 1 meter. Therefore, it is recommended that people maintain at least 1 meter of distance [3]–[5]. The physical distancing combined with other actions such as wearing face masks, avoiding crowded places, and home quarantine are effective measures to reduce the spreading of COVID-19 [6], [7]. Those are also believed to prevent spreading from other contagious diseases like severe acute respiratory syndrome (SARS) or Middle East Respiratory Syndrome (MERS). Unfortunately, there are not many available instruments like detectors for physical distancing violations to enforce people for adhering to the guidelines and health protocols during the pandemic.

Technological intervention is crucial and significant to reduce COVID-19 transmissions. Artificial intelligence (AI) technology is exploited to analyze aspects of the pandemic from contact tracing, early detection, and treatment [8]. Besides, AI was also employed to monitor social distancing violations in crowded areas and to detect whether people were wearing face masks or not. However, it might still be in the preliminary stage for physical distancing and need more implementation in public areas.

A camera and computer, namely visual social distancing (VSD), is introduced to estimate inter-personal distance automatically from an image and characterize a related people aggregation [9]. The VSD is also capable of pointing out social behavior in the scene. Some other works [10], [11] also implemented computer vision to monitor physical distancing violations. Those works employed a graphical processing unit (GPU) and some advanced algorithms such as You Only Look Once (YOLO), YOLO-Tiny, and Single Shot Detector (SSD). Although computer vision has promising prospects, it requires complex signal processing and additional hardware due to the heavy computational burden for processing an image. Besides

computer vision-based, proximity sensor-based on an oscillating magnetic field has also been reported to solve physical distancing violations. This technique was successfully tested in the laboratory and the real world by wearing the sensor at the body to detect a closer person [12]. However, this technique has a low range detection, and it is only for personal usage. The sensor used is the only one that can get the physical distancing violation information. Using this technique will require many sensors to determine whether there is a physical distancing violation in a large and crowded area because each person in that area must wear the sensors. This condition causes a higher total cost and an ineffective application procedure. Therefore, a low-cost physical distancing detector that monitors a large area is needed.

Several distance sensors, such as ultrasonic-based or optical-based sensors, can be exploited to build a physical distancing detector. Many researchers have been developing these sensors to offer many benefits, especially contactless with measured objects. Compared with ultrasonic-based sensors, distance sensors with optical-based offer improved performance for long distances, rapid detection, and better recognition between two objects [13]. This makes optical-based sensors become a promising prospect among available distance sensors. One popular distance sensor with optical based is Lidar (short for light detection and ranging).

Lidar operates with a simple working principle by counting a time difference between transmitted light and reflected light for calculating a distance [14], [15]. Many established methods are now being used to count the time difference at lidar technology. Like radar (short for Radio Detection and Ranging), frequency modulated continuous wave (FMCW) and time of flight (ToF) both can be applied to modulate light source for calculating time delay between transmitted and reflected light. Time delay is needed to range an object which is a target in applications. Despite FMCW offering better resolution and longer distance coverage [14], ToF lidar is now still well known in the market due to its simple operation and cost-effectiveness.

This paper introduces a simple and cost-effective physical distancing violation detector design by applying a single ToF lidar mounted on the stepper motor. We tested our system to detect three dummy objects with various configurations. Using our system, we succeed in measuring a distance object to Lidar and rotation scan and then determining a physical distance between objects using a simple vector operation. We then analyzed performance, such as predicting a dimension of the object and showing a simulation safe and unsafe distance when applied to enforce health protocols during the pandemic. We also implemented our system to detect a physical distance between three persons in the indoor environment. In this demonstration, we achieved measured physical distance between two close person is nearly equal to the configuration.

II. MATERIALS AND METHOD

A. Working Principle of ToF Lidar

At least, ToF lidar is constructed from a light source, photodetector, lenses, and signal modulator. Many light sources can be used in lidars, such as light-emitting diode (LED), laser, and camera. Wavelength, power, and beam divergence are key parameters in the selection of light sources.

Of course, considering selection from parameters has its own advantages and drawbacks between performances and cost. Choosing a photodetector should be matched with the selected wavelength from the light source in the lidar constructions. Usually, a photodetector with material from Ge, Si, InGaAs, and InGaAsP is used to detect a reflected optical signal from a target and convert it into an electrical signal [16]. Lenses are also an important part of Lidar. Diameter and focus length should be well-selected before being attached to the light source and photodetector. A pulse or continuous wave from a signal generator is usually used to modulate the intensity of the light source in ToF lidar.

Consequently, different type of modulation signal causes different techniques on how to calculate the round-trip time of light to travel from light source to a target and then back reflected the photodetector. There are two types of ToF lidar: direct and indirect-ToF. In direct-ToF, it is usually exploited a pulse signal to modulate the light source. On the other hand, an indirect-ToF method usually utilizes a continuous wave signal for modulating light sources [17], [18].

The working principle of direct-ToF lidar measurement is illustrated in Fig. 1. The light source emits a short pulse with high optical power toward an object and is back reflected to the photodetector. Distance (d) is simply by computing from round trip time of the pulse. An electronic timer or time digital converter (TDC) is usually used to calculate the pulse's round-trip time. Counting a time starts when a pulse is emitted from the light source and stops when the photodetector receives a pulse. Thereby, the distance of the object can be calculated by using Eq. (1):

$$d = c\frac{T}{2} \qquad (1)$$

where T is the round-trip time of pulse and c is the speed of light. This method has some advantages: simple, fast, accurate, and not elaborate [19], [20]. Compared to indirect ToF, direct-ToF can be applied for a much longer distance due to no ambiguity when ranging an object [21], [22].
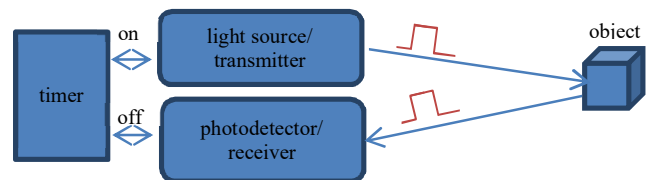

Fig. 1 The working principle of direct-ToF Lidar

Although direct-ToF Lidar has many advantages, it also has some drawbacks, such as the high power of pulsed laser to obtain a sufficient signal-to-noise ratio (SNR). Moreover, obtaining a millimeter resolution requires a very short pulse and picoseconds resolution electronic timer or TDC. Therefore, direct-ToF Lidar is complicated and costly to implement. Another approach called indirect-ToF was proposed by estimating a delay time between transmitted and received signal using phase shift of modulated light with either a sinusoidal or pulsed signal [23]–[25]. The basic principle of indirect-ToF Lidar can be seen in Fig. 2. The distance (d) of the object can be estimated by using Eq. (2).

$$d = \frac{c}{4\pi f}\varphi \qquad (2)$$

where f is modulated frequency and φ is a phase shift between transmitted and received modulated signal [26]. Resolution and maximum range depend on frequency modulation. High-frequency modulation is used to obtain higher resolution. However, it causes a limited shorter measurable distance. Many researchers involve multi-tone of modulation signals to resolve that problem for getting better resolution and longer distance [27].
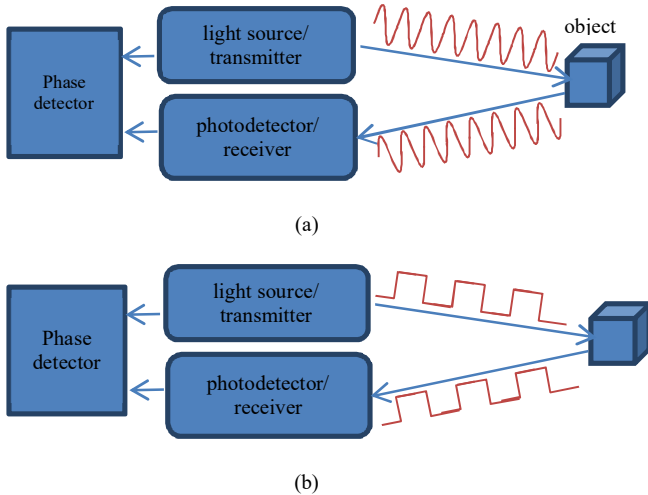

(a)

(b)

Fig. 2 The basic principle of indirect-ToF (a) using sinusoudal wave and (b) square wave.
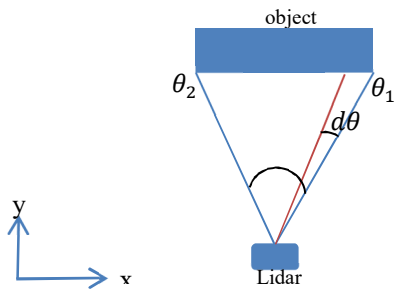

Fig. 3 The illustration of FOV in Lidar

The other important aspect of lidar technology is a field of view (FOV), which is a span of the area that Lidar can observe. FOV is represented in degrees and depicted in Fig. 3. The Lidar shown in Fig. 3 has FOV by θ_2-θ_1 and an angular resolution by dθ. Various Lidar in the available market has FOV from 40 to 360 degrees, depending on their applications. The angular resolution is mainly influenced by a system on how to move the Lidar. The smaller angular resolution helps a lidar to obtain a high profile of the object. Thus, several methods have been applied to enhance FOV and angular resolution, such as by scanner, mirror, MEMS, and motor [28].

B. Detector Set-Up

The Block diagram of the physical distancing violation detector is shown in Fig. 4. We use a ToF lidar from Benewake with an operating range of 0.3 to 12 m and a resolution of 5 mm [29]. Light is transmitted from the Lidar to the target to detect an object. Then it is back reflected to the photodetector, converted to distance information, and then sent by serial communication. The ToF Lidar is placed on a stepper motor using a sensor mount. The stepper motor is

employed to drive the ToF Lidar for rotating up to 180 degrees around in a horizontal plane. A microcontroller controls the stepper motor's rotational scan and steps direction by sending a pulse through a motor driver. This enables reading simultaneously the distance from ToF lidar to target and the magnitude of the stepper motor's rotational scan. The step resolution of the stepper motor is 0.2 degrees. By rotating the Lidar with the stepper motor, our system can detect and evaluate the object that is located in front of the Lidar. All the data are collected by the microcontroller and then analyzed using a personal computer, programmed using LabView software.
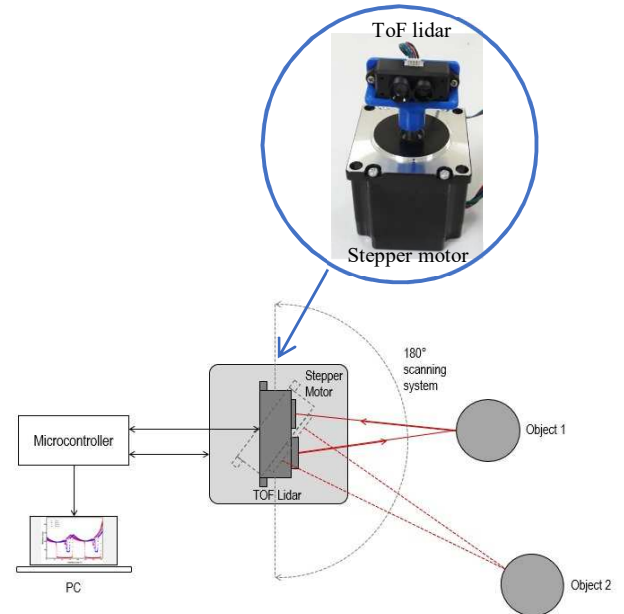

Fig. 4 Schematic set up of physical distancing violation detector based on ToF lidar

C. Physical Distance Estimation Using Vector Operation

We adopt a simple vector operation constructed by two vectors and the angle formed by the intersection between them to determine the physical distance between two objects. Two objects are put in front of the detector, as described in Fig. 5. We then place the Lidar at a center point (O). Let l_1 and l_2 be the measured distances from O to object 1 and object 2, respectively, and an angle Θ is an intersection angle formed by vector l_1 and l_2. The angle Θ corresponds to the rotation scan angle of Lidar in our system. Therefore, it is straightforward to determine the distance between object 1 and object 2 using Eq. (3).

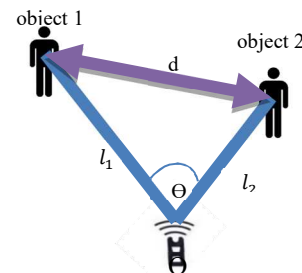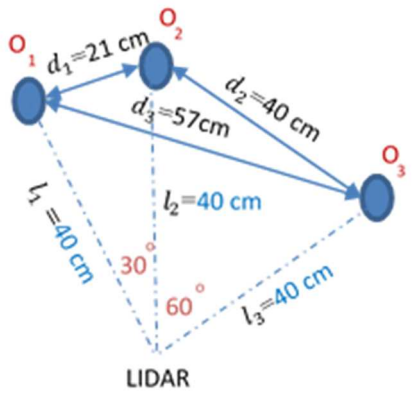$$d = \sqrt{{l_1}^2 + {l_2}^2 - 2l_1 l_2 \cos\theta} \qquad (3)$$

Fig. 5 Illustration of how to define physical distancing between two objects using vector operation
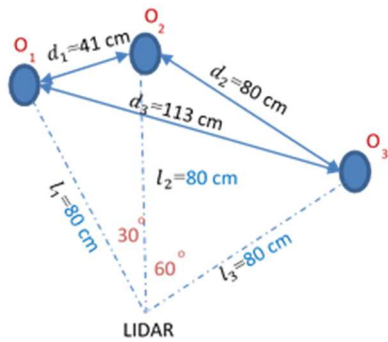
III. RESULTS AND DISCUSSION

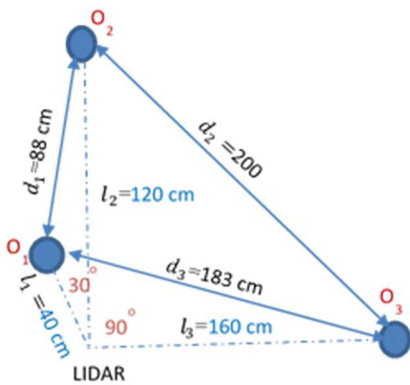### A. Distance Measurement of The Target from Cylinder Tube

We first demonstrated our system to measure the target's distance as a dummy in an indoor environment. We tested on 3 identical observed objects (O_1, O_2, and O_3) with cylinder tube having a diameter of 13 cm and height of 13 cm; then placed them with different distance and intersection angle as shown in Fig. 6. The scenario on how to put the objects is carried out as follows. Factual distances of the observed object to Lidar are notated by l_n, factual distances between two observed objects are notated by d_n, and factual angle θ_n is formed by intersection from two observed objects with respect to Lidar. Using our system, l_n can be measured by Lidar, and then θ_n can be recorded from angular movement of the stepper motor. In Fig. 6(a) and 6(b), we configured an angle between two objects with respect to Lidar at 30° and 60°; In other hands, Fig. 6(c) and 6(d) with an angle of 30° and 90°.
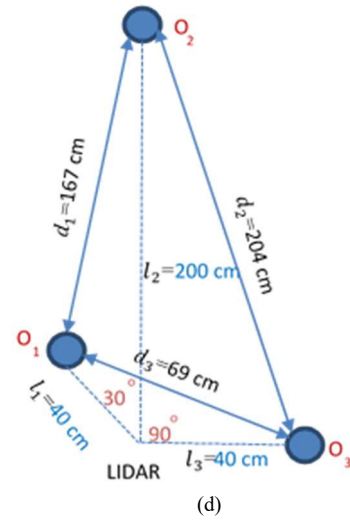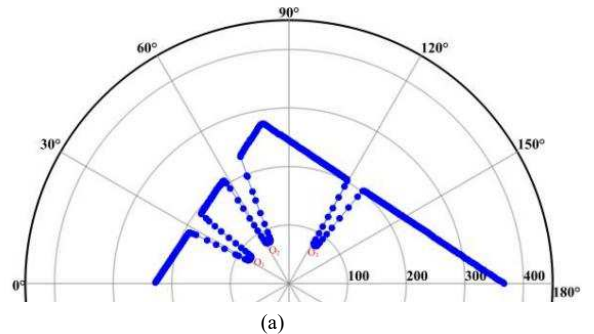

(d)

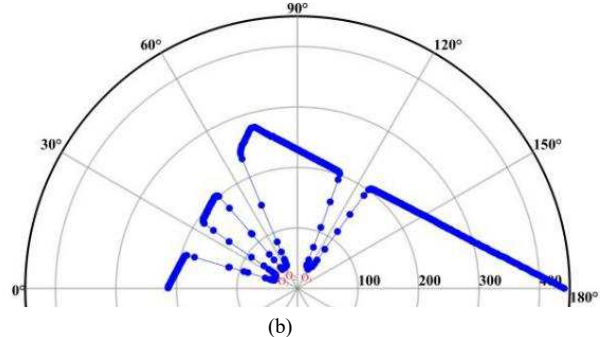Fig. 1 Configuration of measurement 3 objects by using our system with l_n and θ_n: (a) 40 cm, 40 cm, 40cm, 30°, and 60° (b) 80 cm, 80 cm, 80cm, 30°, and 60° (c) 40 cm, 120 cm, 160cm, 30°, and 90° (d) 40 cm, 200 cm, 40cm, 30°, and 90°.

The measurements from the configurations given in Fig. 6 are depicted in Fig. 7. We plot recorded data into polar coordinates, and we find three facets corresponding to 3 detected objects with labels O_1, O_2, and O_3. To convince those 3 facets to correlate to the observed objects, we also consider measuring the background, as pointed out in Fig. 8. Because there are no objects in Fig. 8, a straight line and no facet compared with Fig. 7. It also shows that the straight line that makes 1 corner in Fig. 7 and Fig. 8 represents the wall, which is the borderline in the indoor environment, as can be seen in a photo in Fig. 9.
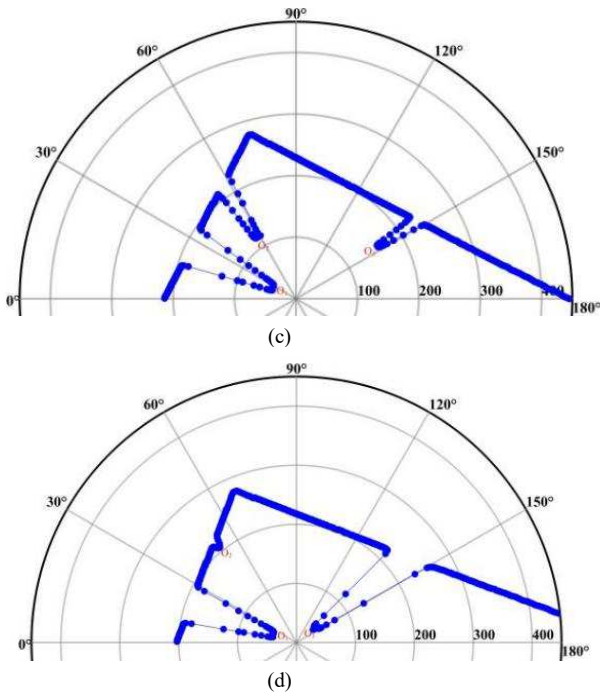

(a)

(b)

(a)

(b)

(c)

1076

(c)

(d)

Fig. 2 Lidar range data recorded of 3 observed objects with the configuration of l_n and θ_n: (a) 60 cm, 60 cm, 60 cm, 30°, and 60°, (b) 80 cm, 80 cm, 80 cm, 30°, and 60°, (c) 40 cm, 120 cm, 160 cm, 30°, and 90°, (d) 40 cm, 200 cm, 40 cm, 30°, and 90°.
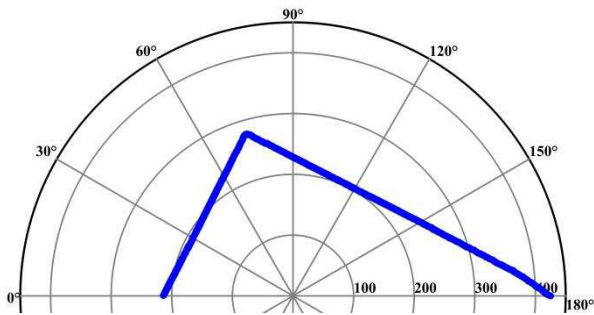

Fig. 8 Lidar range data recorded when no object.

Fig. 3 Photo of measurement objects and surrounding environment

To verify the results, we compare factual and measured data. To distinguish the real and measured data, we define the measured distance with l'_n and rotation scan with θ'_n. The recorded data are summarized in Table I and then processed by following these steps. For instance, we try to retrieve the graph in Fig. 7(a) into Cartesian coordinate as shown in Fig. 10, so we get l'_n at x-axis and θ'_n at y-axis. To calculate l'_n and θ'_n, we introduce a centroid, which a center of recorded data defines is taken from rotation scan when meeting a facet. Hence, we can find three centroids from Fig. 10. As a result,

we can calculate l'_n by pulling a virtual line from centroid to x-axis, and θ'_n can be determined by centroid to other centroids. To give an illustration, in Fig. 10, l'_1 is a measured distance of O_1, we obtain 41 cm. Meanwhile, θ'_n is calculated from the centroid of O_1 to centroid O_2, we thus obtain θ'_1 of 32.51°. Like the previous illustration, we also define l'_n and θ'_n for Fig. 7 (b), 7(c), and 7(d). Thus, we can calculate the measured distance (d'_n) between observed object by using Eq. (3) from l'_n and θ'_n. The results are shown in Table II.

TABLE I
MEASURED DATA FROM FIG. 10

Measured distance (cm)			Measured rotation scan (°)		
l'_1	l'_1	l'_1	θ'_1	θ'_2	θ'_3
41	40	36	32.5	59.6	92.1
78	78	81	30.7	60.4	91,1
42	118	159	31.3	89.9	121.2
42	208	37	31.2	92.0	123.2

l'_1 = measured distance O_1 to Lidar, l'_2 = measured distance O_2 to Lidar, l'_3 = measured distance O_3 to Lidar, θ'_1= measured angle between O_1 to O_2, θ'_2= measured angle between O_2 to O_3, $\theta'_3=\theta'_{1+}\theta'_2$ is the measured angle between O_1 to O_3.
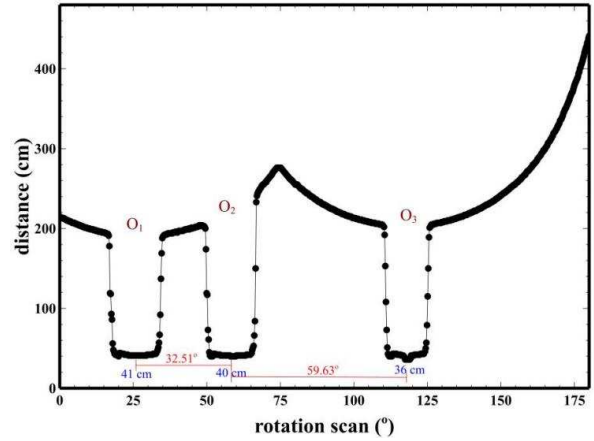

Fig. 4 Plotting data of Fig. 7 (a) in Cartesian coordinate

TABLE II
COMPARISON OF FACTUAL AND MEASURED DISTANCE BETWEEN TWO OBJECTS

Factual distance (cm)			Measured distance (cm)		
d_1	d_2	d_3	d'_1	d'_2	d'_3
21	40	57	23	38	56
41	80	113*	41	80	114*
88	200*	183*	85	198*	184*
167*	204*	69	173*	213*	70

d_1= factual distance between O_1 and O_2, d_2= factual distance between O_2 and O_3, d_3= factual distance between O_1 and O_3, d'_1= measured distance between O_1 and O_2, d'_2= measured distance between O_2 and O_3, d'_3= measured distance between O_1 and O_3, * indicates for a safe distance.

Table II also indicates unsafe and safe distance with the label (*) if we assume the safe distance is more than 100 cm, as recommended by WHO. Although the measured distance is slightly different from the configuration, as shown in Table II, the indicator shown by using the label safe and unsafe still matches factual data. Our system employed a lidar with a resolution of 5 mm and 4 to 6 cm [29]. It might be enough for low-resolution applications like physical distancing violations.

Then, we discuss the vision capability of our system to range the object. In this test, we placed two observed objects (similar to the previous object) with various distances of 40 cm, 80 cm, 120 cm, and 160 cm from Lidar. Instead of plotting into a polar coordinate, we plot our results into a Cartesian coordinate, as shown in Fig. 11. We can see at this graph that when the object is located close to the Lidar, the facets seem wider than the object located far from Lidar. It might be similar to the working principle of the human eye in perspective viewing in the real world. This effect can be well understood by illustrating in Fig. 12. Like as earlier described, l_n' is defined by measured distance by Lidar, and $\Delta\acute{\theta}_n$ is determined as integration from rotation scan when meeting with a surface of the detected object. Therefore, we can estimate the surface of the detected object (s_n) by using Eq. (4).

$$s_n = 2l_n \tan \Delta\theta_n \qquad (1)$$

Table III shows that s_n has nearly 13 cm, which is represented by the object's diameter as described above. However, it might be a problem if an object located far from Lidar due to the resolution of the stepper motor as represented by $\Delta\acute{\theta}_n$. As we can see again in Table III when the object is located further away from Lidar, then $\Delta\acute{\theta}_n$ becomes smaller. Consequently, the object will be difficult to be detected. To solve this problem, it is recommended to select a better resolution for the scanning system when it applies the system located far from the object.
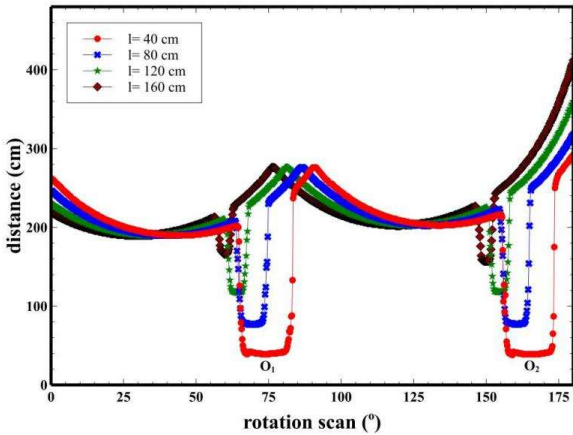

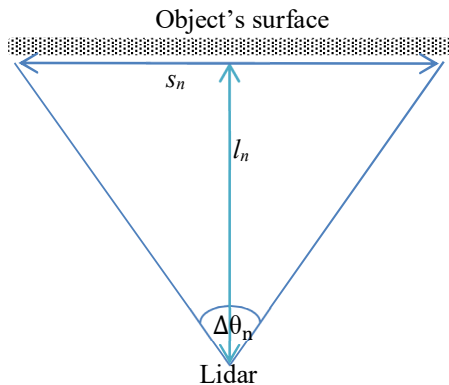Fig. 5 Plotting data of O_1 and O_2 with various distances from Lidar.

Fig. 6 Illustration of estimating dimension of an object from Lidar.

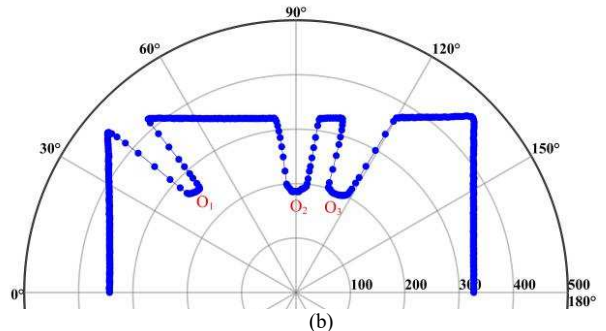| ID	l_1' (cm)	$\Delta\acute{\theta}_1$ (º)	s_1 (cm)	l_2' (cm)	$\Delta\acute{\theta}_2$(cm)	s_2 (cm)
1.	39	18.45	12.67	39	17.77	12.19
2.	77	10.57	14.25	78	9.68	13.21
3.	117	6.75	13.80	118	5.17	14.40
4.	166	4.5	13.04	157	5.17	14.18

1= O_1 and O_2 located 40 cm, 2= O_1 and O_2 located 80 cm, 3= O_1 and O_2 located 120 cm, 4= O_1 and O_2 located 160 cm.

B. Physical Distance Measurement of the people

Lastly, we applied our system to measure the actual physical distances among people. In this experiment, three volunteers stood with 200 cm and 80 cm distances, as shown in Fig. 13(a). Similar to the previous experiment using cylinder tubes, we also succeeded in detecting people with three facets, as pointed out in Fig. 13(b). By using recorded data as l_n' and $\acute{\theta}_n$, we then determine the measured physical distances among them by recalling Eq. (3). Then, we obtain the distance between volunteer 1 to volunteer 2 as 186.5 cm and the distance between volunteer 2 to volunteer 3 as 73.0 cm. This result reveals that volunteer 1 at a safe position, whereas volunteers 2 and 3 might be at risk of spreading contagious diseases if we take recommendations from WHO and CDC.

(a)

(b)

Fig. 7 Measurement a physical distance between person (a) Photo when measurement (b) result measurement.

IV. CONCLUSION

We have developed a simple and low-cost physical distancing violation detector using a rotated ToF lidar and stepper motor. We also successfully implemented our system to measure the distances among the objects, whether dummy objects or real people. Our system offers a cost-effective physical distancing violation detector that employs only ToF Lidar and stepper motor. Besides, our system is simpler because adopting vector operation to define the physical distances. In practical applications, our system might support installing at fixed locations, i.e., parks and supermarkets, and

portable instrument services like security patrol cars and aerial drones.

REFERENCES

[1] World Health Organization, "WHO announces COVID-19 outbreak a pandemic," Mar. 12, 2020. https://www.euro.who.int/en/health-topics/health-emergencies/coronavirus-covid-19/news/news/2020/3/who-announces-covid-19-outbreak-a-pandemic (accessed Mar. 13, 2022).

[2] WHO, "Coronavirus disease (COVID- 19): How is it transmitted?," 2021. [Online]. Available: https://www.who.int/news-room/q-a-detail/coronavirus-disease-covid-19-how-is-it-transmitted. [Accessed: 21-Jan-2020].

[3] IDSA, "Physical Distancing," 2020. [Online]. Available: https://www.idsociety.org/covid-19-real-time-learning-network/infection-prevention/physical-distancing/. [Accessed: 21-Jan-2020].

[4] WHO, "COVID-19: physical distancing," 2021. [Online]. Available: https://www.who.int/westernpacific/emergencies/covid-19/information/physical-distancing#:~:text=Physical distancing helps limit the,Protect yourself and others. [Accessed: 21-Jan-2021].

[5] D. K. Chu et al., "Physical distancing, face masks, and eye protection to prevent person-to-person transmission of SARS-CoV-2 and COVID-19 : a systematic review and meta-analysis," Lancet, vol. 395, no. June, pp. 1973–1987, 2020.

[6] N. M. Ferguson, D. Laydon, G. Nedjati-gilani, N. Imai, K. Ainslie, and M. Baguelin, "Report 9 : Impact of non-pharmaceutical interventions (NPIs) to reduce COVID-19 mortality and healthcare demand," 2020.

[7] M. W. Fong et al., "Nonpharmaceutical Measures for Pandemic Influenza in Nonhealthcare Settings — Social Distancing Measures," Emerg. Infect. Dis., vol. 26, no. 5, pp. 976–984, 2020.

[8] E. Arulprakash and M. Aruldoss, "A Study on Fight Against COVID - 19 from Latest Technological Intervention," SN Comput. Sci., vol. 1, no. 5, pp. 1–3, 2020.

[9] M. Cristani, A. Del Bue, V. Murino, F. Setti, and A. Vinciarelli, "The visual social distancing problem," IEEE Access, vol. 8, pp. 126876–126886, 2020.

[10] S. Suryadi, E. Kurniawan, H. Adinanta, B. H. Sirenden, J. A. Prakosa, and P. Purwowibowo, "On the Comparison of Social Distancing Violation Detectors with Graphical Processing Unit Support," in Proceeding - 2020 International Conference on Radar, Antenna, Microwave, Electronics and Telecommunications, ICRAMET 2020, 2020, pp. 337–342.

[11] H. Adinanta, E. Kurniawan, Suryadi, and J. A. Prakosa, "Physical Distancing Monitoring with Background Subtraction Methods," in Proceeding - 2020 International Conference on Radar, Antenna, Microwave, Electronics and Telecommunications, ICRAMET 2020, 2020, pp. 45–50.

[12] S. Bian, B. Zhou, and P. Lukowicz, "Social distance monitor with a wearable magnetic field proximity sensor," Sensors, vol. 20, no. 18, pp. 1–26, 2020.

[13] G. M. Williams, "Optimization of eyesafe avalanche photodiode lidar for automobile safety and autonomous navigation systems," Opt. Eng., vol. 56, no. 3, pp. 1–9, 2017.

[14] S. Royo and M. Ballesta-Garcia, "An overview of lidar imaging systems for autonomous vehicles," Appl. Sci., vol. 9, no. 19, pp. 1–37, 2019.

[15] C. Li, Q. Chen, G. Gu, and W. Qian, "Laser time-of-flight measurement based on time-delay estimation and fitting correction," Opt. Eng., vol. 52, no. 7, p. 076105, 2013.

[16] C. Rablau, "LIDAR - A new (self-driving) vehicle for introducing optics to broader engineering and non-engineering audiences," in Proc of SPIE, 2019, vol. 11143, no. July 2019, pp. 1–14.

[17] I.-G. Jang, S.-H. Lee, and Y.-H. Park, "A parallel-phase demodulation-based distance-measurement method using dual-frequency modulation," Appl. Sci., vol. 10, no. 1, pp. 1–15, 2020.

[18] D. Bronzi, Y. Zou, F. Villa, S. Tisa, A. Tosi, and F. Zappa, "Automotive Three-Dimensional Vision Through a Single-Photon Counting SPAD Camera," IEEE Trans. Intell. Transp. Syst., vol. 17, no. 3, pp. 782–795, 2016.

[19] T. Fersch, R. Weigel, and A. Koelpin, "A CDMA Modulation Technique for Automotive Time-of-Flight LiDAR Systems," IEEE Sens. J., vol. 17, no. 11, pp. 3507–3516, 2017.

[20] A. Ronchini Ximenes, P. Padmanabhan, M. J. Lee, Y. Yamashita, D. N. Yaung, and E. Charbon, "A Modular, Direct Time-of-Flight Depth Sensor in 45/65-nm 3-D-Stacked CMOS Technology," IEEE J. Solid-State Circuits, vol. 54, no. 11, pp. 3203–3214, 2019.

[21] A. Tontini, L. Gasparini, and M. Perenzoni, "Numerical model of spad-based direct time-of-flight flash lidar CMOS image sensors," Sensors, vol. 20, no. 18, pp. 1–19, 2020.

[22] P. Padmanabhan, C. Zhang, and E. Charbon, "Modeling and Analysis of a Direct Time-of-Flight Sensor Architecture for LiDAR Applications," Sensors, vol. 19, no. 5464, pp. 1–27, 2019.

[23] J. Jang, S. Hwnag, and K. Park, "Design of Indirect Time-of-Flight Based Lidar for Precise Three-Dimensional Measurement Under Various Reflection Conditions," in Proceedings of the 4th International Conference on Sensor Device Technologies and Applications Design, 2013, pp. 25–29.

[24] J.-H. P. Sung-Woo Lee, Haesoo Jeong, Seoung-Ki Lee, Young-Kweon Kim, "LIDAR system using indirect time of flight method and MEMS scanner for distance measurement," in 2016 International Conference on Optical Mems and Nanophotonics (OMN), 2016, pp. 31–32.

[25] S. H. Chung, S. W. Lee, S. K. Lee, and J. H. Park, "LIDAR system with electromagnetic two-axis scanning micromirror based on indirect time-of-flight method," Micro Nano Syst. Lett., vol. 7, no. 1, pp. 4–8, 2019.

[26] S. Bellisai, F. Villa, S. Tisa, D. Bronzi, and F. Zappa, "Indirect time-of-flight 3D ranging based on SPADs," in Proceedings of SPIE, 2012, vol. 8268, pp. 1–8.

[27] M. M. Bayer, R. Torun, I. U. Zaman, and O. Boyraz, "Multi-tone continuous wave lidar in simultaneous ranging and velocimetry," Opt. Express, vol. 28, no. 12, pp. 17241–17252, 2020.

[28] T. Raj, F. H. Hashim, A. B. Huddin, M. F. Ibrahim, and A. Hussain, "A survey on LiDAR scanning mechanisms," Electronics, vol. 9, no. 5, pp. 1–25, 2020.

[29] Benewake, "Product Manual of TFmini," Beijing, 2018.